

Loss of Osteopontin Expression Reduces HSV-1-Induced Corneal Opacity

Adrian Filiberti,¹ Grzegorz B. Gmyrek,¹ Micaela L. Montgomery,² Renee Sallack,¹ and Daniel J. J. Carr^{1,2}

¹Dean McGee Eye Institute, Department of Ophthalmology, University of Oklahoma, Oklahoma City, Oklahoma, United States

²Department of Microbiology and Immunology, University of Oklahoma Health Sciences Center, Oklahoma City, Oklahoma, United States

Correspondence: Daniel J.J. Carr, Dean McGee Eye Institute, Department of Ophthalmology, University of Oklahoma, Acers Pavilion Room 415, 608 Stanton L. Young Boulevard, Oklahoma City, OK 73104, USA; Dan-Carr@ouhsc.edu.

Received: March 26, 2020

Accepted: July 20, 2020

Published: August 12, 2020

Citation: Filiberti A, Gmyrek GB, Montgomery ML, Sallack R, Carr DJJ. Loss of osteopontin expression reduces HSV-1-induced corneal opacity. *Invest Ophthalmol Vis Sci.* 2020;61(10):24. <https://doi.org/10.1167/iovs.61.10.24>

PURPOSE. Corneal opacity and neovascularization (NV) are often described as outcomes of severe herpes simplex virus type 1 (HSV-1) infection. The current study investigated the role of colony-stimulating factor 1 receptor (CSF1R)⁺ cells and soluble factors in the progression of HSV-1-induced corneal NV and opacity.

METHODS. MaFIA mice were infected with 500 plaque-forming units of HSV-1 in the cornea following scarification. From day 10 to day 13 post-infection (pi), mice were treated with 40 µg/day of AP20187 (macrophage ablation) or vehicle intraperitoneally. For osteopontin (OPN) neutralization experiments, C57BL/6 mice were infected as above and treated with 2 µg of goat anti-mouse OPN or isotypic control IgG subconjunctivally every 2 days from day 4 to day 12 pi. Mice were euthanized on day 14 pi, and tissue was processed for immunohistochemistry to quantify NV and opacity by confocal microscopy and absorbance or detection of pro- and anti-angiogenic and inflammatory factors and cells by suspension array analysis and flow cytometry, respectively.

RESULTS. In the absence of CSF1R⁺ cells, HSV-1-induced blood and lymphatic vessel growth was muted. These results correlated with a loss in fibroblast growth factor type 2 (FGF-2) and an increase in OPN expression in the infected cornea. However, a reduction in OPN expression in mice did not alter corneal NV but significantly reduced opacity.

CONCLUSIONS. Our data suggest that CSF1R⁺ cell depletion results in a significant reduction in HSV-1-induced corneal NV that correlates with the loss of FGF-2 expression. A reduction in OPN expression was aligned with a significant drop in opacity associated with reduced corneal collagen disruption.

Keywords: HSV-1, neovascularization, cornea, opacity, osteopontin

The cornea is a highly differentiated tissue characterized in healthy conditions by its transparency.¹ To minimize light scattering, the central cornea aspect has several anatomical and physiological specializations that include unmyelinated nerve fibers, the absence of melanocytes, and the absence of blood and lymphatic vessels. The avascular state of the cornea is maintained through a combination of anti-angiogenic factors including, but not limited to, endostatin, thrombospondin, and tissue inhibitor proteinase-3, as well as other anti-angiogenic factors and decoy receptors for pro-angiogenic molecules.²⁻⁴ It is well documented that corneal neovascularization (NV), including de novo blood and lymphatic vessel genesis, occurs during wound healing, tumorigenesis, and infection. Each of these conditions can result in inflammation with the rapid expression of cytokines and chemokines and subsequent recruitment of immune cells.³

Herpes simplex virus type 1 (HSV-1) infection elicits corneal NV through the upregulation of vascular endothelial growth factor (VEGF)-A initially by resident epithelial

cells⁵ and perhaps neutrophils that infiltrate the cornea in response to infection.⁶ In addition, HSV-1 induces the expression of the cognate receptors (VEGFR-2 and VEGFR-3) for VEGF-A on the newly acquired lymphatic vessels.⁷ The upregulation of VEGF-A following infection is mediated through the HSV-1-encoded immediate-early gene product infected cell protein-4.⁵ However, the process of VEGF-A upregulation occurs well before the development of vessel genesis in the cornea proper. In fact, viral clearance occurs prior to robust corneal NV. Other factors that have been linked to viral-mediated corneal NV during acute infection include IL-6 and TNF-α.^{8,9} Following the clearance of virus, the expression of numerous pro-angiogenic factors peaks at around day 14 post-infection (pi) and subsequently dissipates with the exception of matrix metalloproteinase (MMP)-9 and fibroblast growth factor (FGF)-2.¹⁰ Whereas there remains controversy as to the role of MMP-9 in HSV-1-induced NV,^{10,11} neutralization of FGF-2 has been found to block NV and dampen the expression of other factors associated with angiogenesis, including IL-6, VEGF-A,

hepatocyte growth factor (HGF), and angiopoietin (ANG)-2.¹⁰ The role that these factors have in the generation of new blood and lymphatic vessels in the cornea relative to the infiltration of leukocytes during the progression and maintenance phase of the pathologic process has not been fully elucidated. Based on depletion studies we previously reported, neutrophils (Ly6G⁺Ly6C^{mid}) are not involved in NV during the progression and maintenance phase of vessel growth.¹⁰ However, other inflammatory cells including macrophages, have not been fully evaluated in this process.

Because macrophages contribute to NV as a source of pro-angiogenic factors or as a physical extension to the tube-like vasculature,^{12–15} we investigated the role these cells may have in the progression phase of NV following HSV-1 infection. The results of this study suggest that colony-stimulating factor 1 receptor (CSF1R)-expressing cells (predominantly macrophages and a subpopulation of neutrophils) significantly contribute to the progression of corneal lymphatic and blood vessels following virus infection. Concomitant with CSF1R⁺ cell depletion, we observed a downregulation of FGF-2 and upregulation of osteopontin (OPN). A reduction in OPN levels was found to significantly reduce opacity, and this observation was independent of NV but associated with an increase in MMP-8 expression.

METHODS

Animals

All animal procedures were approved by the University of Oklahoma Health Sciences Center and Dean McGee Eye Institute Institutional Animal Use and Care Committee and were performed in adherence to the ARVO Statement for the Use of Animals in Ophthalmic and Vision Research. Macrophage Fas-induced apoptosis (MaFIA) transgenic mice (stock number 005070 on a C57BL/6 background expanded as a colony at the Dean McGee Eye Institute vivarium), and C57BL/6 wild-type (WT) mice (stock number 000664) were obtained from The Jackson Laboratory (Bar Harbor, ME, USA). Mice were 7 to 10 weeks old at the time of performing experiments. Prior to scarification, harvesting tissue, or euthanizing animals, mice were deeply anesthetized with ketamine (100 mg/kg) and xylazine (6.6 mg/kg). Animals were euthanized by cardiac perfusion with 10 mL PBS.

Virus and Infection

HSV-1 strain McKrae was propagated in green monkey kidney (Vero) cells and maintained at a stock concentration of 1.7×10^8 to 1.0×10^9 plaque-forming units (PFU)/mL. Anesthetized mice were infected by scarification of the corneal surface with a 25-G 1.5-inch needle and tear film blotted, followed by application of 2.0 μ L of RPMI medium containing virus (500 PFU/eye) as previously described.¹⁶ Non-infected control animals included scarification of corneas only.

Treatment with B/B Homodimerizer

Forty micrograms of the compound AP20187 B/B homodimerizer (AP, catalog no. 635058, lot no. 1902029; Takara Bio USA, Mountain View, CA, USA) or vehicle (VEH) solution (4% ethanol, 10% PEG-400, and 1.7% Tween 80 in sterile water) was intraperitoneally injected into MaFIA transgenic mice daily for 4 consecutive days, starting at

day 10 pi as previously described.^{17,18} Treatment of mice depletes CSF1R-expressing cells in circulation, as well as in the cornea of infected mice.^{17–19}

Treatment with Anti-Mouse OPN Antibody

Starting at day 4 pi, anesthetized WT mice received subconjunctival injections of 2 μ g (in 2 μ L of sterile PBS) of goat anti-mouse OPN IgG (catalog no. AF808, lot no. BDO0618021; R&D Systems, Minneapolis, MN, USA) or normal goat IgG (catalog no. AB-108-C, lot no. ES4119031; R&D Systems) as isotypic control using a 31-gauge syringe under a dissecting scope. Injections were repeated every 2 days through day 12 pi, and mice were euthanized at day 14 pi.

Immunohistochemistry and Imaging

Mice were euthanized and the eyes were removed at the indicated time post-infection. All tissue preparation, antibody sources and dilutions, and confocal imaging were as previously described.¹⁹ For each cornea, each of four quadrants was analyzed.

Protein Extraction, Angiogenic Proteome Profile, and Suspension Array

Corneas were harvested and homogenized in sterile PBS containing protease inhibitors—10 μ g/mL aprotinin (catalog no. A6279; Sigma-Aldrich, Natick, MA, USA), 10 μ g/mL leupeptin (catalog no. 1167; Tocris Bioscience, Bristol, UK), and 10 μ g/mL pepstatin (catalog no. 1190; Tocris)—using 1.5-mL snap-cap Eppendorf tubes (Advanced Bullet Blender Storm 24 (Troy, NY, USA)), three times for 5 minutes each at the maximum setting. Samples were then centrifuged (1 minute, 10,000g), and the protein content in the clarified supernatant was quantified using a Pierce BCA Protein Assay Kit (catalog no. 23227; Thermo Fisher Scientific, Waltham, MA, USA).

The proteome profile was performed using a mouse angiogenesis proteome array according to the manufacturer's recommendations (catalog no. ARY015; R&D Systems). The relative intensity of the blots was quantified using the open-source platform for biological image analysis, Image J software (National Institutes of Health, Bethesda, MD, USA). Mouse Magnetic Luminex Assays (catalog no. MMMP1MAG-79K; EMD Millipore, Burlington, MA, USA) were used to quantify pro-/anti-angiogenic factors, including Serpin-E1, FGF-2, VEGF-A, tissue inhibitor of metalloproteinase-1 (TIMP-1), OPN, and insulin-like growth factor binding protein (IGFBP)-3, according to the manufacturer's instructions (catalog no. LXSAMSM; R&D Systems). Metalloproteinase (MMP)-2, MMP-3, and MMP-8 levels were detected using Mouse Magnetic Luminex Assays (EMD Millipore). IL-1 α , IL-6, CXCL1, and CCL2 levels were determined using Magnetic Luminex Assays (catalog no. 12002798; Bio-Rad Laboratories, Hercules, CA, USA). The concentration of each candidate protein is expressed as pg analyte/mg total protein.

Corneal Opacity Measurement and Collagen Stain

Corneas were harvested from infected or uninfected MaFIA and WT mice and fixed with 4% paraformaldehyde for

30 minutes at room temperature followed by washing in 1 mL PBS 3×, 10 minutes per wash. Corneas were then immersed in glycerol 50% in PBS for 30 minutes. Each cornea was placed in the bottom and center of the well of a 96-well, U-bottom plate. The remaining glycerol was removed, and the corneas were then incubated at room temperature for 10 minutes. At that time, 50 μ L of PBS was added to each well, and the tissue was assayed for absorbance at 500 nm in the FLUOstar Omega (BMG LABTECH, Offenburg, Germany).

To measure denatured collagen strands, corneas were permeabilized and washed as previously described¹⁹ and placed separately in the bottom of the well of a 96-well, U-bottom plate. The wells were then placed on ice, and 20 μ L of 20- μ M biotinylated collagen hybridizing peptide (B-CHP; 3Helix, Salt Lake City, UT, USA) was added to each cornea followed by overnight incubation at 4°C. Corneas were then washed three times in 1 mL PBS (10 minutes per wash) and incubated overnight at 4°C with Alexa Fluor 647 conjugated with streptavidin (3.85 μ g/mL; Jackson ImmunoResearch, West Grove, PA, USA). Prior to mounting, the corneas were washed as described above (three times in PBS, 30 minutes each wash). The corneas were mounted in 50% glycerol and imaged using an Olympus FluoView confocal laser scanning microscope (Olympus Corporation, Center Valley, PA, USA).

Flow Cytometry and Cell Sorting

The extracted corneas harvested from MaFIA mice were exposed to Liberase TL (catalog no. 05401020001; Roche, Mannheim, Germany) for 30 minutes at 37°C at the indicated time point post-infection. Digested tissue was filtered through a 40- μ m cell strainer and washed with staining buffer (PBS supplemented with 2% FBS). Single cell suspensions were treated with CD16/CD32 Ab (clone 93) for 10 minutes at 4°C to block nonspecific binding and then stained for 20 minutes on ice with a combination of fluorochrome-conjugated antibodies (all from BioLegend, San Diego, CA, USA): CD45 (clone 30-F11), CCR2 (clone SA203G11), CD64 (clone X54-5/7.1), CD206 (clone C068C2), and major histocompatibility complex (MHC) class II (clone M5/114.15.2). The final gate was set on infiltrating macrophages defined as CD45⁺GFP⁺CD64⁺CCR2⁺, followed by analysis of cell subsets expressing CD206 and/or MHCII. Data were acquired on a MACSQuant Analyzer Flow Cytometer (Miltenyi Biotec, Auburn CA, USA) and analyzed with FlowJo software.

To further establish the subpopulations of myeloid and T-lymphocyte populations that were depleted in MaFIA mice following AP20187 homodimerizer treatment, a second series of labeling was conducted. Single-cell cornea suspensions were treated with CD16/CD32 Ab (clone 93) for 10 minutes at 4°C to block nonspecific binding and then stained for 20 minutes on ice with a combination of fluorochrome-conjugated antibodies (all from BioLegend): CD45 (clone 30-F11), CCR2 (clone SA203G11), CD11b (clone M1/70), Ly6G (clone 1A8), and Ly6C (clone H1.4), with the addition of GFP^{+/-} gate to separate CSF1R-expressing and non-expressing cells, or with a combination of fluorochrome-conjugated antibodies including CD45 (clone 30-F11; BioLegend), CD3 (clone 145-2C11; BioLegend), CD4 (clone GK1.5; BioLegend), and CD8a (clone 53-6.7; Thermo Fisher Scientific). Data acquisition and analysis were identical as described above.

A Sorter S3e (Bio-Rad Laboratories) equipped with a 488-nm, 100-mW laser was used for all myeloid cell-sorting experiments. The instrument performance (i.e., laser power, fluids flow, and shutter) was controlled by ProSort software, version 1.6 (Bio-Rad Laboratories) working under the Windows operating system (Microsoft Corporation, Redmond, CA, USA). For cell sorting, the instrument was set per the manufacturer's settings using a 100-nm tip nozzle, and drop delay was optimized using Proline Universal Calibration Beads (Bio-Rad Laboratories). Compensation and gates were set based on fluorescence collected through a 488/560 bandpass filter. All cell-sorting experiments used pooled cells isolated from corneas after enzymatic digestion (four to six mice per one cell-sorting experiment). The cells were filtered through 30-nm cell strainers and resuspended in PBS supplemented with 2% FBS. Sorted cell populations were identified as follow: CD45⁺CD11b⁺GFP⁺, CD45⁺CD11b⁺GFP⁻, and CD45⁻Epcam (Epcam/CD326 clone G8.8; BioLegend). All sorting experiments were done under the purity sort mode. The efficiency of cell sorting across all experiments ranged between 95% and 100%. Epcam⁺ cells were enriched as previously described.²⁰

Statistical Analysis

Data are presented as mean \pm SEM. Prism 5 software (GraphPad, San Diego, CA, USA) was used for statistical analysis, and tests utilized are described in each figure legend. Data were considered to be significant at $P < 0.05$.

RESULTS

CD45⁺CD11b⁺GFP⁺ Cell Depletion Significantly Reduced HSV-1-Induced Corneal Neovascularization

Macrophages have been noted in the peripheral and central aspects of the cornea stroma of mice.²¹ As macrophages are an evolving population of cells, especially during times of inflammation, we evaluated this population over the course of acute infection to day 21 pi. The results show a significant rise in the CD64⁺CD206⁻ macrophage population at day 7 pi that resolved by day 21 pi (Figs. 1A, 1B). By comparison, the activated CD64⁺CD206⁺ macrophage population levels peaked at day 14 pi and subsequently resolved by day 21 pi (Fig. 1B). Because macrophages have been associated with NV,^{22,23} we next determined whether a loss in the macrophage population that infiltrates the cornea would alter the course of HSV-1-mediated corneal NV. MaFIA transgenic C57BL/6 mice were infected with HSV-1 and subsequently treated with vehicle or AP20187 daily for 4 consecutive days starting 10 days pi to deplete CD45⁺CD11b⁺CSF1R(GFP)⁺ cells from the cornea. This treatment regimen led to the loss of over 92 \pm 2% of GFP⁺ cells in the infected cornea (Fig. 2A) and resulted in a significant drop out of blood and lymphatic vessels found in the cornea proper by day 14 pi (Figs. 2B, 2C). The loss was most pronounced in the blood vasculature, but lymphatic vessels were affected as well.

To confirm the assumption that the majority of the CSF1R⁺GFP⁺ cells were consistent with a macrophage phenotype, flow cytometry analysis was conducted on VEH- and AP20187-treated mouse cornea single-cell suspensions. The results show that there was no loss in

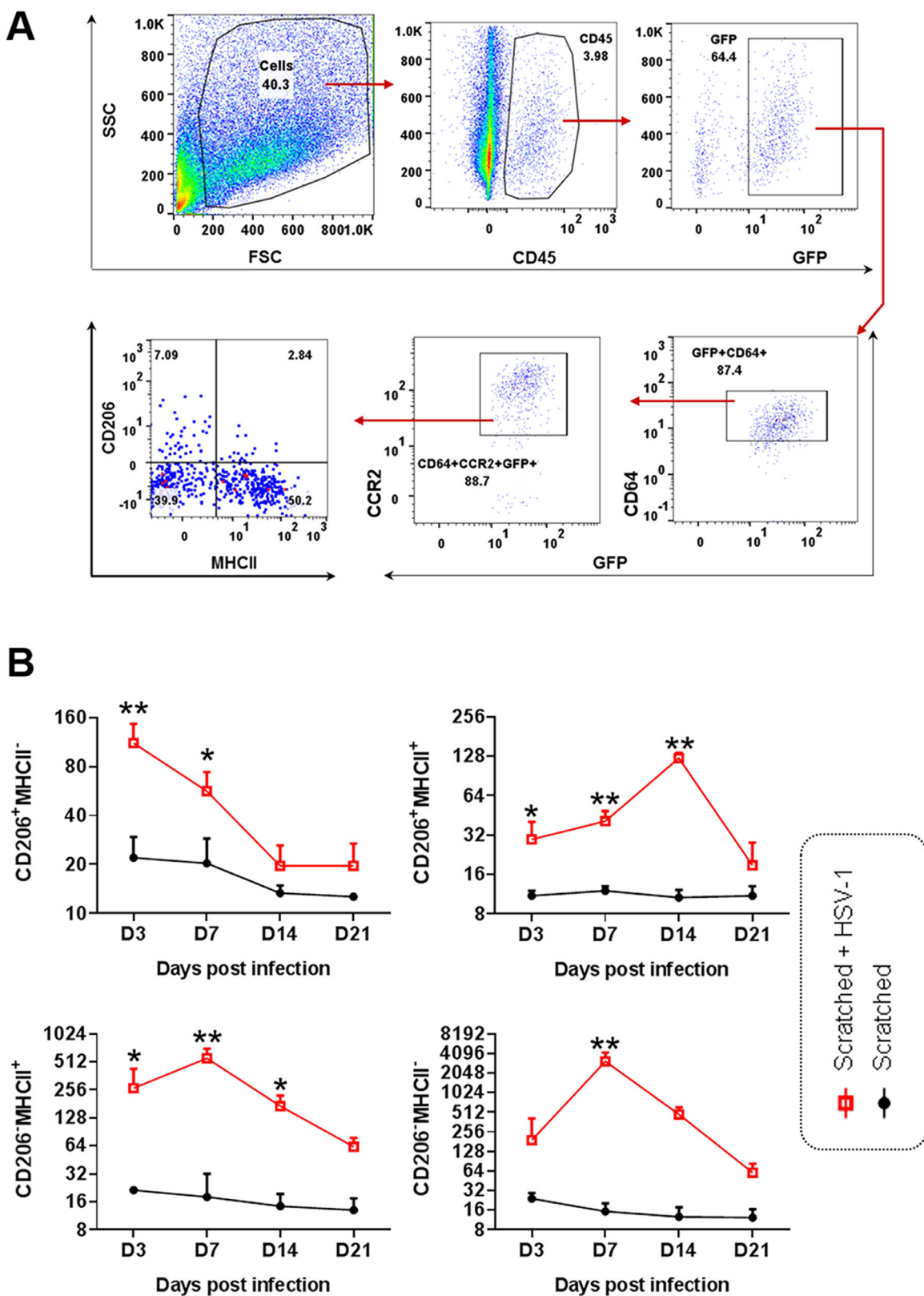


FIGURE 1. Changes in dynamics in macrophage subsets infiltrating the cornea after HSV-1 infection. The corneas from MaFIA mice were infected following scarification with HSV-1 (500 PFU/cornea). At day (D) 3, D7, D14, and D21 pi, the corneas were harvested and digested with Liberase followed by staining with cocktail antibody sets as described in the Methods section. Stained cells were acquired with flow cytometry and analyzed with FlowJo software. (A) Representative image of the gating strategy (corresponding to day 3 pi). (B) Distribution pattern of macrophage subsets at the indicated time points. The values are presented as mean \pm SEM from two experiments with three mice per group for each time point. Scratched mouse corneas that were not infected served as controls. ** $P < 0.01$, * $P < 0.05$ comparing the indicated group to the scarified control group as determined by Student's *t*-test and Holm-Sidak correction.

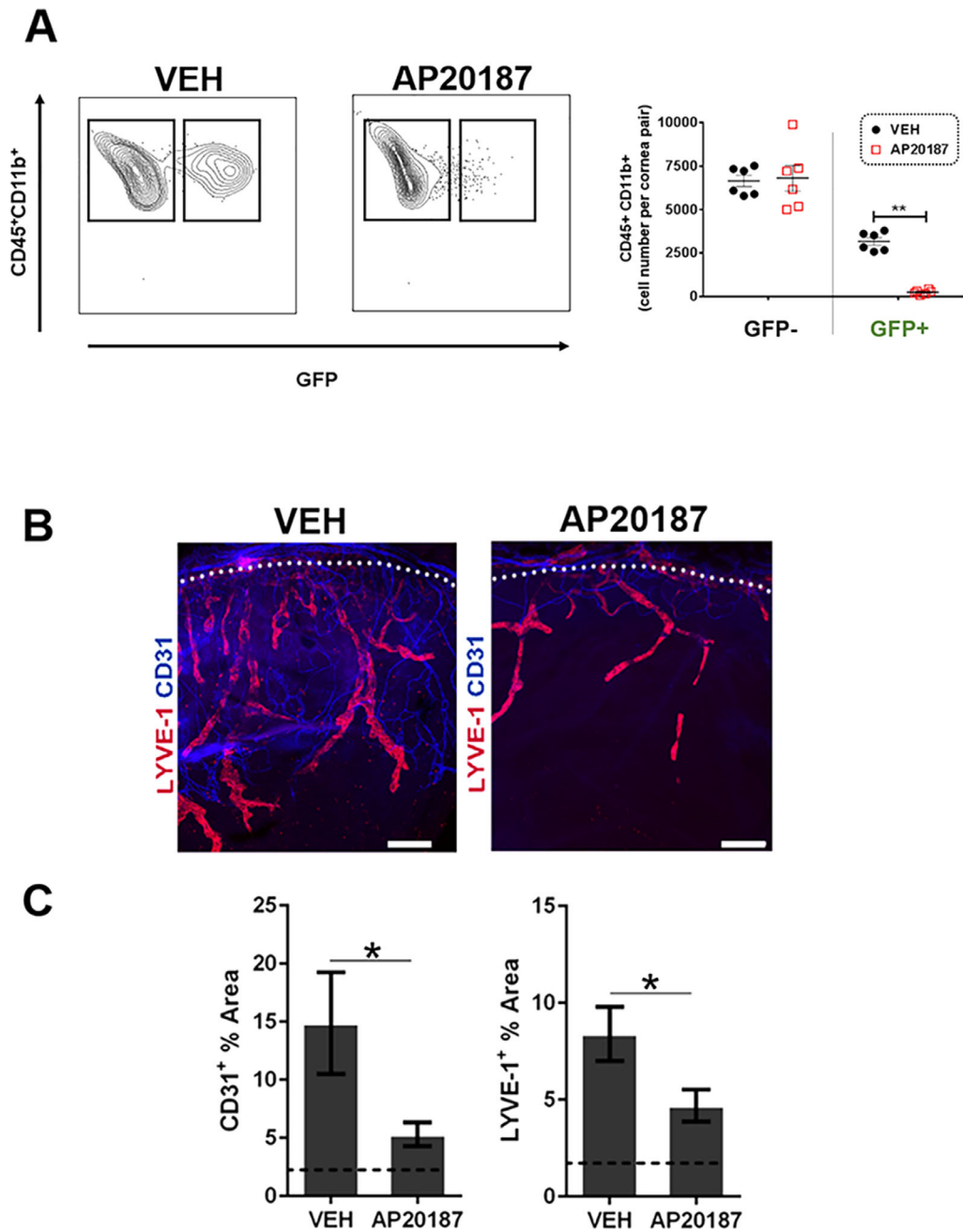


FIGURE 2. Depletion of CSF1R⁺ cells resulted in a loss of HSV-1-induced neovascularization in the cornea of MaFIA mice. MaFIA mice were infected with HSV-1 (500 PFU/eye) and treated with AP20187 dimerizer or vehicle control as described in the Methods section. **(A)** Representative flow cytometry plot comparing CSF1R⁺ GFP⁺ cells after AP20187 and VEH treatment in the cornea day 14 pi. Summary of two experiments depicting depletion of GFP⁺ cells following AP20187 treatment. ***P* < 0.001 comparing the VEH- to AP20187-treated groups as determined by Student's *t*-test and Holm–Sidak correction (*n* = 6 per treatment). **(B)** Representative confocal microscopy images of whole-mount cornea at day 14 pi from mice treated with VEH or AP20187 (scale bar: 100 μm). Blue, blood vessels (CD31⁺); red, lymphatic vessels (LYVE-1⁺); *discontinuous white line*, corneoscleral limbus margins. Each image represents a z-stack quadrant of a cornea. **(C)** Metamorph quantification of the cornea area containing blood (CD31⁺) or lymphatic (LYVE-1⁺) vessels presented as mean + SEM (*n* = 5 corneas per treatment). **P* < 0.05 comparing the VEH- to AP20187-treated group as determined by Student's *t*-test.

the neutrophil (CD45⁺CD11b⁺Ly6G⁺Ly6C^{mid}CCR2^{+/-}) or inflammatory monocyte/macrophage (CD45⁺CD11b⁺Ly6G⁺Ly6C^{high}CCR2^{+/-}) GFP⁻ cell populations that reside in the cornea of HSV-1-infected mice comparing VEH- to AP20187-treated groups (Figs. 3A, 3B; Supplementary Figs. S1, S2). This group constitutes the majority (68%) of the myeloid (CD11b⁺) cell population that resides

in the cornea at day 14 pi. However, in the GFP⁺ cell population that constituted 30% of the myeloid cells residing in the cornea of infected mice, AP20187 treatment depleted these cells, which included macrophages (CD45⁺CD11b⁺Ly6G⁻Ly6C^{high}CCR2^{+/-}) and neutrophils (CD45⁺CD11b⁺Ly6G⁺Ly6C^{mid}CCR2^{+/-}) (Figs. 3C, 3D). Of note, the remaining fraction of CD45⁺CD11b⁺ cells not

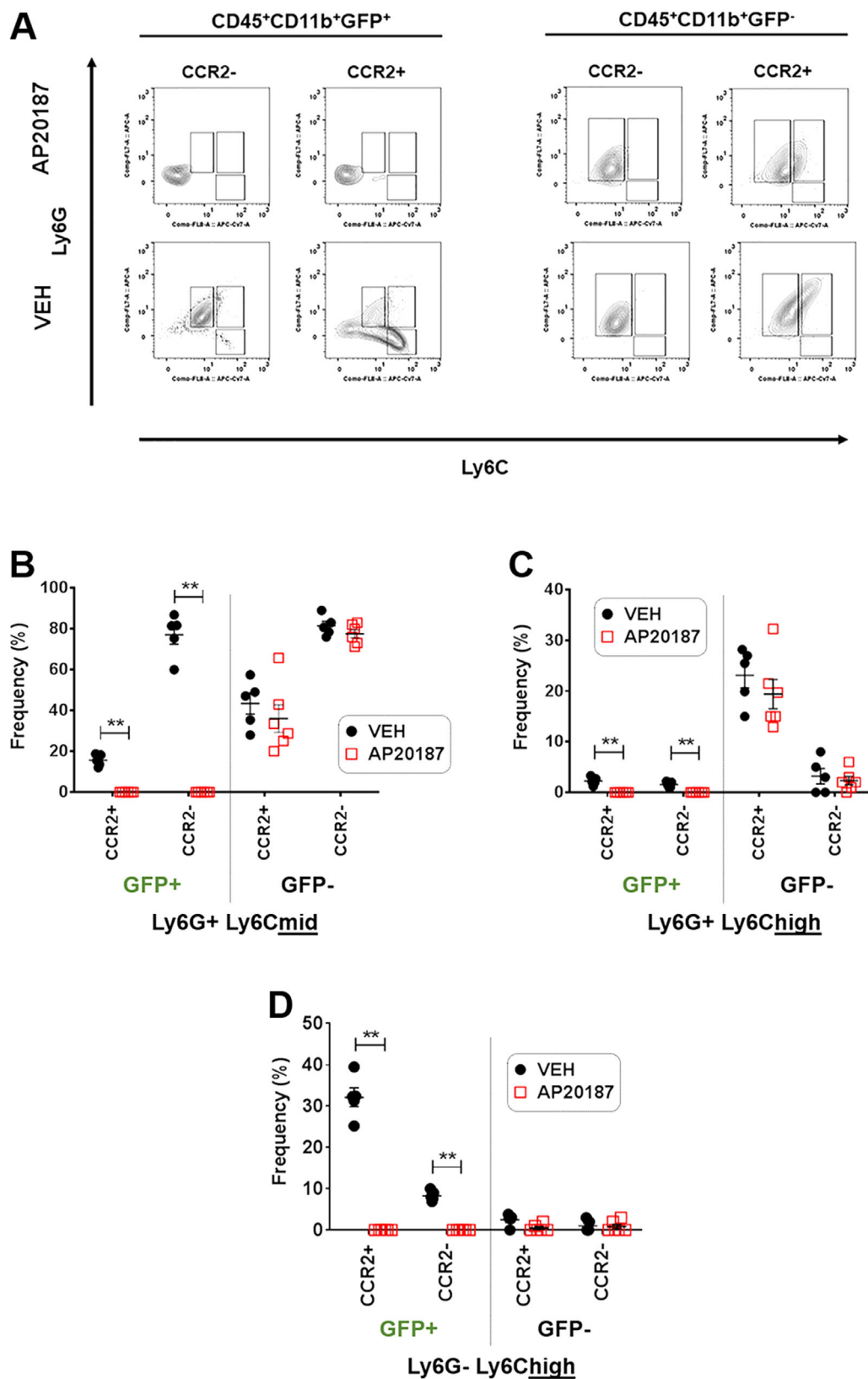


FIGURE 3. Depletion of CSF1R (GFP⁺) cells resulted in a significant loss of macrophages and a unique population of neutrophils. MaFIA mice were infected with HSV-1 (500 PFU/eye) and treated with AP20187 dimerizer or vehicle control as described in the Methods section. (A) Representative flow cytometry plot comparing CD45⁺CD11b⁺CSF1R⁺ GFP⁺ and CD45⁺CD11b⁺CSF1R⁻ GFP⁻ cells and expression of CCR2 after AP20187 and VEH treatment in the cornea day 14 pi. (B–D) Summary of data represented in A for (B) GFP⁺ neutrophils (Ly6G⁺Ly6C^{mid}), (C) GFP⁺ inflammatory monocytes (Ly6G⁺Ly6C^{high}), and (D) GFP⁻ macrophages (Ly6G⁻Ly6C^{high}). ***P* < 0.001 comparing the VEH- to AP20187-treated groups for each phenotype as determined by Student's *t*-test and Holm–Sidak correction.

depleted expressed very low levels of Ly6G and displayed a high side scatter profile consistent with a granulocyte/neutrophil cell, but exactly what these cells constitute remains an enigma. A second analysis was conducted on the T-lymphocyte populations to determine whether unexpected changes occurred with these cells post-AP20187 treatment. Similar to GFP⁺ myeloid populations, there were no differences in the frequency of CD4⁺ or CD8⁺ T cells comparing VEH-treated to AP20187-treated HSV-1-infected MaFIA mice (Supplementary Fig. S3).

CD45⁺CD11b⁺CSF1R⁺ Cell Depletion in Cornea Resulted in Significant Decrease in FGF-2 and Increase in OPN Expression

The relationship between soluble pro-/anti-angiogenic factors is a complex, multivariable, and interactive network. As an initial attempt to identify proteins that contribute to or dampen HSV-1-induced NV in the MaFIA transgenic mouse model, an interactome analysis was conducted using the functional protein association network software STRING (<https://string-db.org/>)²⁴ and the input data of pro- and anti-angiogenic factors including ANG-2, FGF-2, MMP-9, HGF, CCL3, CXCL2, CXCL1, CXCL2, CXCL10, IFN- γ , IL-1, IL-6, IL-10, IL-12, IL-17, IL-18, TNF- α , and VEGF-A.^{9,10,25-35} A total of 187 proteins were identified with pro-/anti-angiogenic properties defined by an interaction confidence score of 0.900 or greater. Candidate proteins included those already identified with a clear role in HSV-1-induced NV including VEGF-A and FGF-2, as well as other proteins with less defined roles, including OPN, IGFBP-3, and ANG-1, among others (Fig. 4A).

To analyze the relative expression profile of the angiogenesis-related proteins in cornea after HSV-1-infection, a mouse proteome angiogenesis profile analysis was performed. The result of this semiquantitative technique found that 14 proteins were downregulated and 16 proteins were upregulated comparing CSF1R⁺-depleted corneas to non-depleted corneas (data not shown). These results gave us a target base for further investigation using a more quantitative means, with the limitation of the availability of reagents to detect select candidate proteins. Based on the results from the semiquantitative mouse proteome angiogenesis profile, six proteins (FGF-2, IGFBP-3, OPN, serpin-E1, TIMP-1, and VEGF-A) were further evaluated to quantify expression in the cornea of MaFIA transgenic mice infected with HSV-1 and treated with AP20187 or VEH. HSV-1-infected mice depleted of macrophages expressed significantly less FGF-2 and, inversely, significantly more OPN compared to the VEH-treated control group at day 14 pi (Fig. 4B). The other four proteins surveyed did not differ significantly between the two groups of MaFIA-treated mice.

To identify the source of the soluble factors expressed following HSV-1 infection, single-cell suspensions of HSV-1-infected corneas were sorted into four highly enriched groups: epithelial cells (CD45⁺EpCam⁺), leukocytes minus CSF1R (CD45⁺GFP⁻), CSF1R-enriched leukocytes (CD45⁺GFP⁺), and stromal fibroblasts and endothelial cells (CD45⁻EpCam⁻). RNA extracted from sorted cell populations was assessed for relative levels of soluble factor transcripts by real-time RT-PCR. Serpin-E1, TIMP-1, and IGFBP-3 were primarily expressed by the stromal cell/endothelial cell populations (Fig. 4C). FGF-2 was expressed in stromal/endothelial cell and macrophage

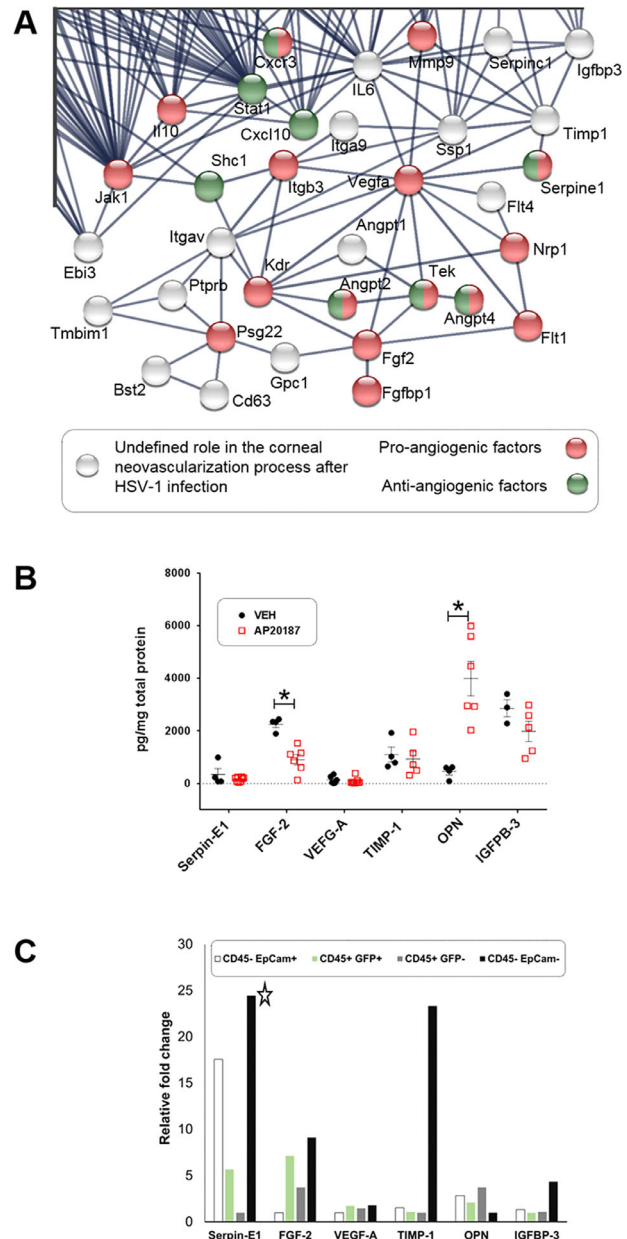


FIGURE 4. Analysis in silico and analytes assayed in vivo. (A) Functional protein association network analysis performed with STRING software. Angiogenic core proteins are included, with molecules involved in various immune system processes excluded. Each node represents one protein produced by a single protein-coding locus. Lines represent protein–protein associations (physical and/or functional association). The biological process associated with these proteins is noted by color: *red*, pro-angiogenic factors; *green*, anti-angiogenic factors; *gray*, undefined role in corneal HSV-1-induced NV. Proteins include the following: Angpt1, angiopoietin-1; Angpt2, angiopoietin-2; Angpt4, angiopoietin-4; Bst2, bone marrow stromal antigen-2; Cd63, CD63 antigen; Cxcr3, C-X-C chemokine receptor type 3; Cxcl10, C-X-C motif chemokine 10; Ebi3, interleukin 27; FGF-2, fibroblast growth factor 2; Fgfbp1, fibroblast growth factor-binding protein-1; Flt1, vascular endothelial growth factor receptor-1; Flt4, vascular endothelial growth factor receptor-3; Gpc1, glypican-1; Igfbp3, insulin-like growth factor-binding protein-3; IL-6, interleukin-6; IL-10, interleukin-10; Itga9, integrin alpha-9; Itgav, integrin alpha-5; Itgb3, integrin beta-3; Jak1, tyrosine-protein kinase-1; Kdr, vascular endothelial growth factor receptor-2; MMP-9, matrix metalloproteinase-9; Nrpl1, neuropilin-1; Psg22, pregnancy-specific glycoprotein-22; Ptpnb, receptor-type tyrosine-protein phosphatase beta; Serpinc1, antithrombin-III; Serpine1, plasminogen

populations, whereas VEGF-A and OPN expression was equally distributed among the enriched cell populations (Fig. 4C).

To evaluate the relationship between OPN and NV, neutralizing antibody to OPN was administered subconjunctivally to mice following infection. Treatment of HSV-1-infected mice with anti-OPN IgG reduced OPN expression by 50% to 60% (Fig. 5A) without affecting other soluble factors measured, including FGF-2, TIMP-1, and IGFBP-3 (data not shown). Furthermore, there was no significant difference in corneal NV comparing anti-OPN IgG to the ISO control-treated group of animals (Fig. 5B).

Reduction in OPN Expression Resulted in Loss of Opacity in the Cornea of HSV-1-Infected Mice

Corneal opacity is a feature often reported in experimental HSV-1 keratitis.^{28,36,37} Although there was no change in corneal NV comparing anti-OPN IgG-treated versus isotypic IgG control-treated eyes infected with HSV-1, there was a noticeable increase in the clarity of the cornea of anti-OPN IgG-treated mice. Using a methodology developed in our lab (Supplementary Fig. S4), we were able to quantify opacity based on absorbance of damaged cornea tissue and found a significant reduction in corneal opacity from mice treated with anti-OPN IgG compared to the isotypic IgG control (Fig. 6A). However, the opacity score was still above uninfected baseline levels. Using a biotin-conjugated collagen hybridizing peptide, denatured collagen foci were readily identified more often and to a greater degree in corneas from isotypic IgG control-treated mice compared to anti-OPN IgG-treated animals (Fig. 6B). To determine whether the loss of CSF1R⁺ cells altered the opacity in HSV-1-infected mice, MaFIA mice were treated with VEH or AP20187 and opacity scores were assessed. The results show that the absence of CSF1R⁺ cells did not alter the corneal opacity of the HSV-1-infected mice (Fig. 6C), suggesting that these cells do not contribute to collagen fiber damage.

MMPs are associated with degradation of collagen, opacity, and ocular HSV-1 infection.^{38–40} Because there was a significant change in the collagen architecture in the cornea of HSV-1-infected mice treated with isotypic control IgG-treated compared to the anti-OPN IgG-treated mice, we investigated MMP levels and inflammatory markers between these two groups. At the time opacity scores were assessed, there was no difference in MMP-2, MMP-3, IL-1 α , IL-6, CCL2, or CXCL1 levels recovered in the cornea of anti-OPN versus isotypic control-treated mice (Figs. 7A, 7B). However, there

activator inhibitor-1; Shc1, SHC-transforming protein-1; Ssp1, osteopontin; Stat1, signal transducer and activator of transcription-1; Tek, angiopoietin-1 receptor; Timp1, metalloproteinase inhibitor-1; Tmbim1, protein lifeguard-3; VEGFA, vascular endothelial growth factor-A. Interaction score confidence = 0.900; number of nodes and edges 187 and 360, respectively (not all shown). The input data for this analysis included 18 pro-/anti-angiogenic proteins involved in corneal neovascularization induced by HSV-1 infection. (B) Protein expression of select analytes obtained from corneal protein extracts from MaFIA mice treated with AP20187 and VEH. **P* < 0.05 by unpaired *t*-test comparing AP20187 to VEH group. (C) Relative fold-change expression of indicated transcripts from sorted corneal cell populations from MaFIA mouse corneas day 14 pi. Corneas from 10 animals were pooled. The asterisk represents the value reduced 20-fold to fit within the range included in the figure.

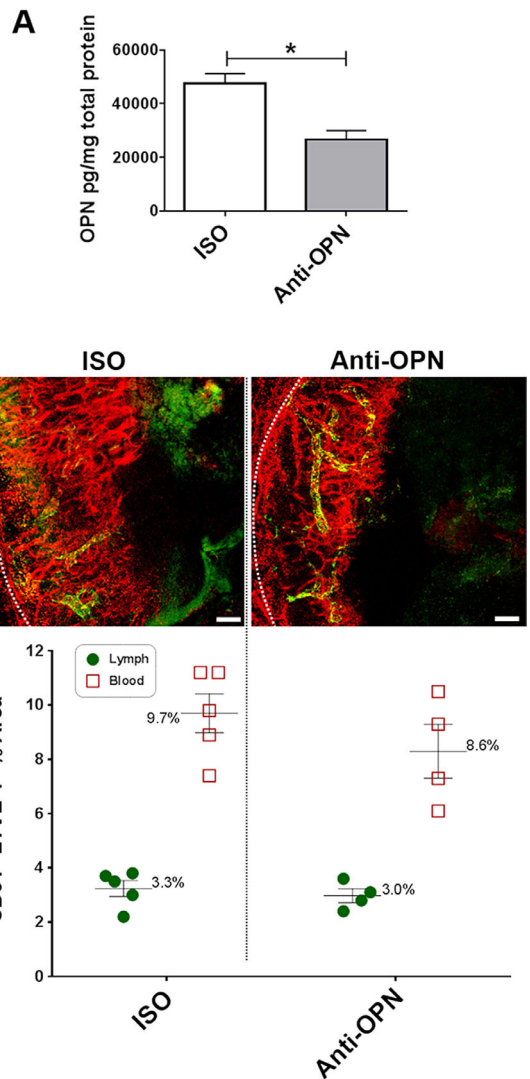


FIGURE 5. Anti-OPN antibody treatment did not affect corneal neovascularization. MaFIA mice were infected with 500 PFU (HSV-1) and treated with anti-OPN or isotypic control (ISO) IgG every 2 days starting at day 4 pi as described in the Methods section. Mice were euthanized at day 14 pi and evaluated for cornea OPN levels by suspension array (A) or corneal neovascularization (B). In A, the results are expressed in picograms of OPN per milligram of total protein. Scale bars depict mean \pm SEM; *n* = 5 per group per experiment, total of two experiments; **P* < 0.05 by two-tailed, unpaired *t*-test corrected using the Holm–Sidak method. In B, the top panel includes a representative confocal microscopy image of flat-mount cornea from each treated group (scale bar: 100 μ m). Red, blood vessels (CD31⁺); green, lymphatic vessels (LYVE-1⁺); discontinuous white lines, corneoscleral limbus margin. The bottom panel is a summary of the percent threshold area positive for blood and lymphatic vessels (CD31⁺ and LYVE-1⁺) \pm SEM (*n* = 5 mice per group).

was a significant increase in MMP-8 found in the cornea of mice treated with anti-OPN IgG (Fig. 7B).

DISCUSSION

Corneal NV is induced by various inflammatory stimuli including microbial pathogens (e.g., HSV-1), corneal transplantation, chemical burns, and ischemia.^{41,42} Experimental models of corneal trauma and HSV-1 infection

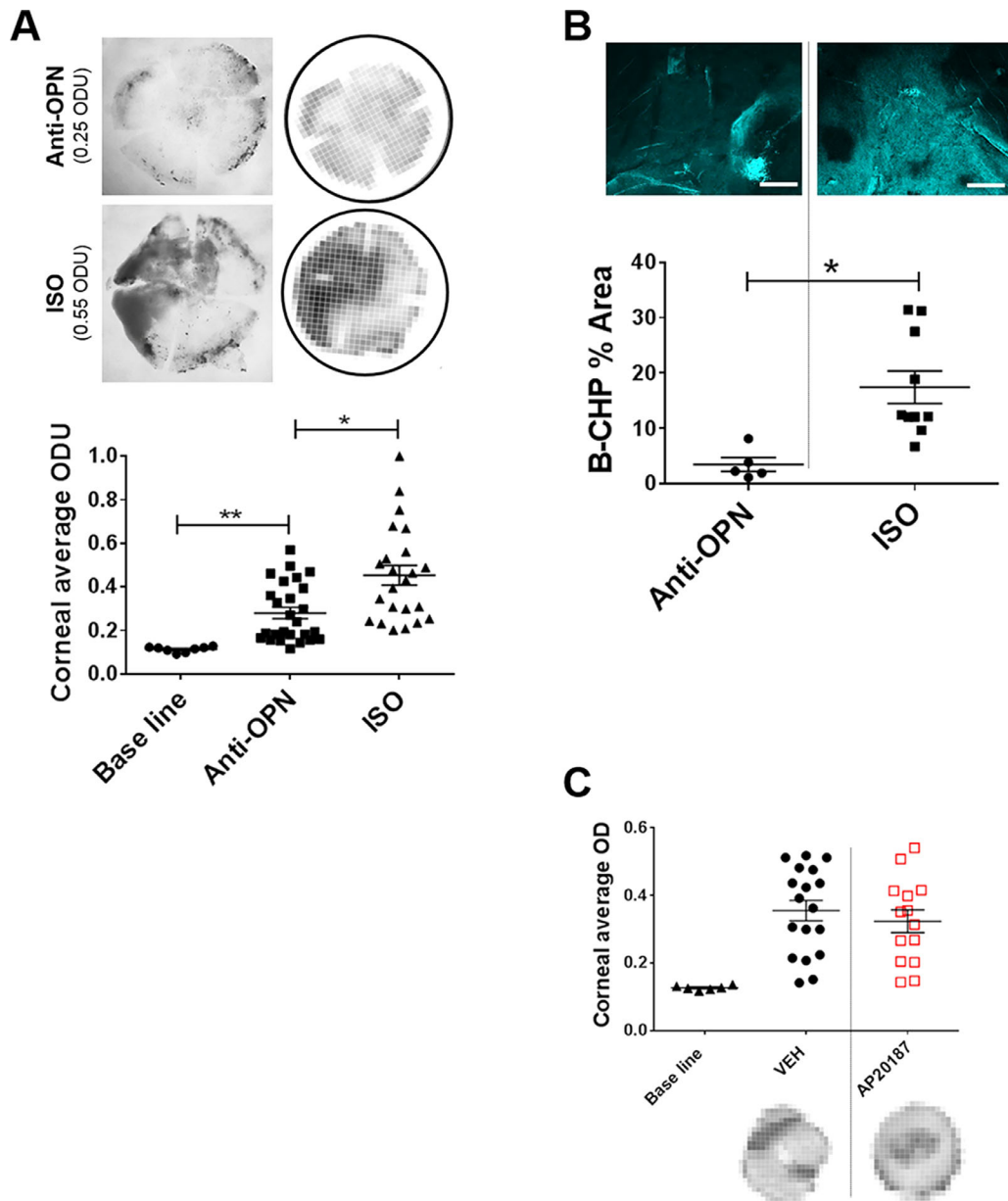


FIGURE 6. Osteopontin neutralization reduced HSV-1-mediated corneal opacity. MaFIA mice were infected with 500 PFU (HSV-1) and treated with anti-OPN or isotypic control (ISO) IgG every 2 days starting at day 4 pi as described in the Methods section. Mice were euthanized at day 14 pi, and the corneas were surgically removed and assessed for opacity measuring the optical density at 500-nm wavelength in a 30-by-30 matrix distributed over the corneal surface. Mouse corneas scarified but not infected served as baseline controls. **(A)** Top panel is representative images (32× magnification) of two corneas treated with anti-OPN or ISO IgG (left) and images (right) digitalized with analyzed optical density units (ODU) of 0.25 and 0.55, respectively. Lower panel is a summary from two experiments of 24 corneas per group displaying the mean (horizontal line) ± SEM corneal ODU. ** $P < 0.0001$, * $P < 0.05$ as determined by two-tailed, unpaired t -test with Holm–Sidak correction. It should be noted that the ISO to baseline control group is also $P < 0.0001$. **(B)** Top panel is a representative confocal microscopy image of flat-mounted corneas from day 14 pi mice treated with anti-OPN or ISO IgG (scale bar: 100 μ m) showing damaged collagen stained with collagen hybridizing peptide biotin conjugated (B-CHP, blue) to detect denatured collagen (see Methods). Horizontal bars depict the mean percent area positive for B-CHP ± SEM. * $P < 0.05$ as determined by two-tailed, unpaired t -test with Holm–Sidak correction. **(C)** The corneas of HSV-1-infected MaFIA mice ($n = 7$ to 9 mice per group) treated with VEH or AP20187 were analyzed for opacity by absorbance measurement at 500 nm day 14 pi. The baseline score of uninfected MaFIA mice is included.

have reported that hem- and lymphangiogenesis are closely linked, and they serve as major routes of induction of adaptive immunity.^{43,44} Central to the initial phase of corneal vessel genesis is VEGF-A, a potent pro-angiogenic factor that primarily promotes blood vessel growth² but has also been reported to be critical to lymphatic vessel genesis in response to HSV-1 infection.⁷ VEGF A has also been reported to recruit circulating Ly6C⁺ monocytes that are

reprogrammed and contribute to remodeling small vessels into large vascular conduits, and they are a significant source of pro-angiogenic factors including VEGF-A, -C, and -D.^{2,45,46}

In the present work, we found that the depletion of CSF1R⁺ cells, including macrophages and a subpopulation of neutrophils, during the progressive phase of NV results in a loss of blood and lymphatic vessels. This change in angiogenesis correlated with a significant reduc-

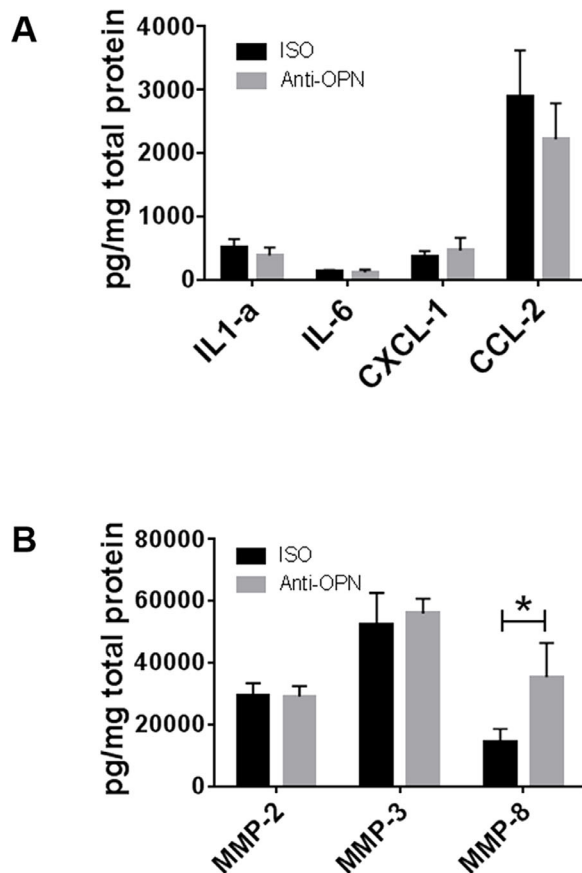


FIGURE 7. Osteopontin neutralization resulted in enhanced MMP8 expression in the cornea. MaFIA mice were infected with 500 PFU (HSV-1) and treated with anti-OPN or isotypic control (ISO) IgG every 2 days starting at day 4 pi as described in the Methods section. Mice were euthanized at day 14 pi, and the corneas were surgically removed and processed for analyte assessment by suspension array. **(A)** Measurement of IL-1 α , IL-6, CXCL1, and CCL2 expressed as mean pg analyte/total cornea protein \pm SEM ($n = 10$ or 11 per group from two independent experiments). **(B)** Measurement of MMP-2, MMP-3, and MMP-8 expressed as mean pg analyte/total cornea protein \pm SEM ($n = 10$ or 11 per group from two independent experiments). * $P < 0.05$ comparing the ISO- to anti-OPN-treated groups as determined by two-tailed, t -test comparison and Holm-Sidak correction.

tion in FGF-2 expression, consistent with our previous findings suggesting that FGF-2 is a critical factor during this time period.¹⁰ Because macrophages are a source of FGF-2 and can cleave matrix-bound FGF-2 produced by corneal epithelial cells, fibroblasts, and endothelial cells,^{47–49} the depletion of macrophages is consistent with the outcome observed in the current dataset. The peak of CD64⁺CD206⁺ macrophages occurred at day 14 pi with the FGF-2 levels recovered in the infected cornea, as these cells are a source of FGF-2.⁴⁸ However, we cannot discount the potential contribution of the unique neutrophil (CD45⁺CD11b⁺Ly6G⁺Ly6C^{mid}CCR2^{+/-}GFP⁺) population to the NV process. The CD64⁺CD206⁺ macrophages were also CCR2⁺, thought to be recruited from circulation during inflammation.⁵⁰ However, the dynamics of macrophage populations and their contribution to ocular tissue pathology and establishment of resistance to HSV-1 infection in the cornea environment continue to unfold. Macrophages and inflammatory monocytes have been identified as a criti-

cal cell population that initially controls cornea HSV-1 infection.^{51,52} Depletion of these cells may not only exacerbate HSV-1 replication and spread but also diminish corneal wound healing.^{53,54} However, manipulating macrophage plasticity in the local environment through the addition of autonomic nervous system ligands during the course of inflammation is a promising development.⁵⁵

OPN is an extracellular matrix protein that greatly influences fibroblast proliferation, migration, and matrix remodeling and is a critical factor in corneal wound healing.⁵⁶ In terms of corneal HSV-1 infection and consistent with our data, a previous study reported that OPN-deficient mice presented with a significant drop in the incidence and severity of herpes stromal keratitis (HSK) following corneal infection out to day 15 pi.⁵⁷ Whereas several factors known to contribute to or correlate with opacity and HSK were evaluated after OPN neutralization, including IL-1 α , IL-6, CXCL1, CCL2, MMPs, and IGFBP-3,^{58–61} MMP-8 was the only factor investigated that changed (increased) following anti-OPN treatment. In general, MMPs are zinc-binding proteolytic enzymes that are involved in degradation and remodeling of the extracellular matrix in tissues, including the cornea.⁶² In the case of MMP-8, one study reported dexamethasone-treated, alkali-injured corneas showed a significant drop in the levels of MMP-1, -9, and -13 and TIMP-1, as well as an increase in MMP-8 expression, that correlated with improved corneal opacity scores.⁶³ Such results may involve a reduction in TGF- β expression as previously reported.⁶⁴ However, the role of OPN in HSV-1-mediated corneal pathology requires further rigorous investigation, as OPN is involved in immune regulation and the expression of various cytokines and chemokines.^{57,65,66}

The lack of a consistent, quantitative means to evaluate corneal opacity has plagued vision science and continues to do so.⁶⁷ Similar to subjective scoring of the cornea for NV, numerous investigative teams assess corneal opacity in terms of grade or score based on visual inspection with or without the aid of a slit-lamp. Although the method reported in the current study is limited in its use to ex vivo analysis, it utilizes a common piece of laboratory equipment in research labs often used to determine absorbance for ELISAs kits. Our analysis of corneas from mice includes a matrix template programmed into the instrument that allows the entire flat-mounted cornea to be assessed in under 10 minutes. We note that, during our analysis, there was no correlation between NV and opacity, as opacity initiated well before signs of NV in response to HSV-1 infection. Such results suggest that, at least in experimental HSV-1 cornea infection, opacity and NV are independent of one another.

Acknowledgments

Supported by grants from the National Institutes of Health (R01 EY021238, P30 EY021725). Additional support was provided by an unrestricted grant from Research to Prevent Blindness.

Disclosure: **A. Filiberti**, None; **G.B. Gmyrek**, None; **M.L. Montgomery**, None; **R. Sallack**, None; **D.J.J. Carr**, None

References

1. DelMonte DW, Kim T. Anatomy and physiology of the cornea. *J Cataract Refract Surg*. 2011;37:588–598.
2. Bock F, Maruyama K, Regenfuss B, et al. Novel anti(lymph)angiogenic treatment strategies for corneal and

- ocular surface diseases. *Prog Retin Eye Res.* 2013;34:89–124.
3. Bryant-Hudson K, Conrady CD, Carr DJ. Type I interferon and lymphangiogenesis in the HSV-1 infected cornea - are they beneficial to the host? *Prog Retin Eye Res.* 2013;36:281–291.
 4. Ambati BK, Nozaki M, Singh N, et al. Corneal avascularity is due to soluble VEGF receptor-1. *Nature.* 2006;443:993–997.
 5. Wuest T, Zheng M, Efstathiou S, Halford WP, Carr DJ. The herpes simplex virus-1 transactivator infected cell protein-4 drives VEGF-A dependent neovascularization. *PLoS Pathogens.* 2011;7:e1002278.
 6. Suryawanshi A, Mulik S, Sharma S, Reddy PB, Sehrawat S, Rouse BT. Ocular neovascularization caused by herpes simplex virus type 1 infection results from breakdown of binding between vascular endothelial growth factor A and its soluble receptor. *J Immunol.* 2011;186:3653–3665.
 7. Wuest TR, Carr DJ. VEGF-A expression by HSV-1-infected cells drives corneal lymphangiogenesis. *J Exp Med.* 2010;207:101–115.
 8. Biswas PS, Banerjee K, Kinchington PR, Rouse BT. Involvement of IL-6 in the paracrine production of VEGF in ocular HSV-1 infection. *Exp Eye Res.* 2006;82:46–54.
 9. Bryant-Hudson KM, Gurung HR, Zheng M, Carr DJ. Tumor necrosis factor alpha and interleukin-6 facilitate corneal lymphangiogenesis in response to herpes simplex virus 1 infection. *J Virol.* 2014;88:14451–14457.
 10. Gurung HR, Carr MM, Bryant K, Chucair-Elliott AJ, Carr DJ. Fibroblast growth factor-2 drives and maintains progressive corneal neovascularization following HSV-1 infection. *Mucosal Immunol.* 2018;11:172–185.
 11. Lee S, Zheng M, Kim B, Rouse BT. Role of matrix metalloproteinase-9 in angiogenesis caused by ocular infection with herpes simplex virus. *J Clin Invest.* 2002;110:1105–1111.
 12. Xu H, Chen M, Reid DM, Forrester JV. LYVE-1-positive macrophages are present in normal murine eyes. *Invest Ophthalmol Vis Sci.* 2007;48:2162–2171.
 13. Maruyama K, Ii M, Cursiefen C, et al. Inflammation-induced lymphangiogenesis in the cornea arises from CD11b-positive macrophages. *J Clin Invest.* 2005;115:2363–2372.
 14. Maruyama K, Nakazawa T, Cursiefen C, et al. The maintenance of lymphatic vessels in the cornea is dependent on the presence of macrophages. *Invest Ophthalmol Vis Sci.* 2012;53:3145–3153.
 15. Cursiefen C, Chen L, Borges LP, et al. VEGF-A stimulates lymphangiogenesis and hemangiogenesis in inflammatory neovascularization via macrophage recruitment. *J Clin Invest.* 2004;113:1040–1050.
 16. Conrady CD, Zheng M, Fitzgerald KA, Liu C, Carr DJ. Resistance to HSV-1 infection in the epithelium resides with the novel innate sensor, IFI-16. *Mucosal Immunol.* 2012;5:173–183.
 17. Burnett SH, Kershen EJ, Zhang J, et al. Conditional macrophage ablation in transgenic mice expressing a Fas-based suicide gene. *J Leukoc Biol.* 2004;75:612–623.
 18. Chinnery HR, Carlson EC, Sun Y, et al. Bone marrow chimeras and c-fms conditional ablation (Mafia) mice reveal an essential role for resident myeloid cells in lipopolysaccharide/TLR4-induced corneal inflammation. *J Immunol.* 2009;182:2738–2744.
 19. Chucair-Elliott AJ, Gurung HR, Carr MM, Carr DJ. Colony stimulating factor-1 receptor expressing cells infiltrating the cornea control corneal nerve degeneration in response to HSV-1 infection. *Invest Ophthalmol Vis Sci.* 2017;58:4670–4682.
 20. Royer DJ, Elliott MH, Le YZ, Carr DJ. Corneal epithelial cells exhibit myeloid characteristics and present antigen via MHC class II. *Invest Ophthalmol Vis Sci.* 2018;59:1512–1522.
 21. Brissette-Storkus CS, Reynolds SM, Lepisto AJ, Hendricks RL. Identification of a novel macrophage population in the normal mouse corneal stroma. *Invest Ophthalmol Vis Sci.* 2002;43:2264–2271.
 22. Polverini PJ, Cotran PS, Gimbrone MA, Jr, Unanue ER. Activated macrophages induce vascular proliferation. *Nature.* 1977;269:804–806.
 23. Leibovich SJ, Polverini PJ, Shepard HM, Wiseman DM, Shively V, Nuseir N. Macrophage-induced angiogenesis is mediated by tumour necrosis factor-alpha. *Nature.* 1987;329:630–632.
 24. Szklarczyk D, Gable AL, Lyon D, et al. STRING v11: protein-protein association networks with increased coverage, supporting functional discovery in genome-wide experimental datasets. *Nucleic Acids Res.* 2019;47:D607–D613.
 25. Yao HW, Chen SH, Li C, Tung YY, Chen SH. Suppression of transcription factor early growth response 1 reduces herpes simplex virus 1-induced corneal disease in mice. *J Virol.* 2012;86:8559–8567.
 26. Kim B, Lee S, Suvas S, Rouse BT. Application of plasmid DNA encoding IL-18 diminishes development of herpetic stromal keratitis by antiangiogenic effects. *J Immunol.* 2005;175:509–516.
 27. Rieck P, Denis J, Peters D, Hartmann C, Pouliquen Y, Courtois Y. Fibroblast growth factor 2, heparin and suramin reduce epithelial ulcer development in experimental HSV-1 keratitis. *Graefes Arch Clin Exp Ophthalmol.* 1997;35:733–740.
 28. Twardy BS, Channappanavar R, Suvas S. Substance P in the corneal stroma regulates the severity of herpetic stromal keratitis lesions. *Invest Ophthalmol Vis Sci.* 2011;52:8604–8613.
 29. Sharma S, Mulik S, Kumar N, Suryawanshi A, Rouse BT. An anti-inflammatory role of VEGFR2/Src kinase inhibitor in herpes simplex virus 1-induced immunopathology. *J Virol.* 2011;85:5995–6007.
 30. Biswas PS, Banerjee K, Kim B, Rouse BT. Mice transgenic for IL-1 receptor antagonist protein are resistant to herpetic stromal keratitis: possible role for IL-1 in herpetic stromal keratitis pathogenesis. *J Immunol.* 2004;172:3736–3744.
 31. Shen M, Tao Y, Feng Y, Liu X, Yuan F, Zhou H. Quantitative proteomic analysis of mice corneal tissues reveals angiogenesis-related proteins involved in corneal neovascularization. *Biochim Biophys Acta.* 2016;1864:787–793.
 32. Rajasagi NK, Bhela S, Varanasi SK, Rouse BT. Front-line science: aspirin-triggered resolvin D1 controls herpes simplex virus-induced corneal immunopathology. *J Leukoc Biol.* 2017;102:1159–1171.
 33. Lee S, Zheng M, Deshpande S, Eo SK, Hamilton TA, Rouse BT. IL-12 suppresses the expression of ocular immunoinflammatory lesions by effects on angiogenesis. *J Leukoc Biol.* 2002;71:469–476.
 34. Hazlett LD, Hendricks RL. Reviews for immune privilege in the year 2010: immune privilege and infection. *Ocul Immunol Inflamm.* 2010;18:237–243.
 35. Cursiefen C. Immune privilege and angiogenic privilege of the cornea. *Chem Immunol Allergy.* 2007;92:50–57.
 36. Minagawa H, Sakai Y, Li Y, Ishibashi T, Inomata H, Mori R. Suppression of infectious virus spread and corneal opacification by the combined use of recombinant interferon beta and interleukin-10 following corneal infection with herpes simplex virus-1 in mice. *Antiviral Res.* 1997;36:99–105.
 37. Rowe AM, Yun H, Hendricks RL. Exposure stress induces reversible corneal graft opacity in recipients with herpes simplex virus-1 infections. *Invest Ophthalmol Vis Sci.* 2017;58:35–41.

38. Yang YN, Bauer D, Wasmuth S, Steuhl KP, Heiligenhaus A. Matrix metalloproteinases (MMP-2 and 9) and tissue inhibitors of matrix metalloproteinases (TIMP-1 and 2) during the course of experimental necrotizing herpetic keratitis. *Exp Eye Res.* 2003;77:227–237.
39. Abdelfattah NS, Amgad M, Zayed AA, Hussein H, Abd El-Baky N. Molecular underpinnings of corneal angiogenesis: advances over the past decade. *Int J Ophthalmol.* 2016;9:768–779.
40. Ke L, Yang Y, Li JW, et al. Modulation of corneal FAK/PI3K/Akt signaling expression and of metalloproteinase-2 and metalloproteinase-9 during the development of herpes simplex keratitis. *Biomed Res Int.* 2019;2019:4143981.
41. Ellenberg D, Azar DT, Hallak JA, et al. Novel aspects of corneal angiogenic and lymphangiogenic privilege. *Prog Retin Eye Res.* 2010;29:208–248.
42. Barbariga M, Vallone F, Mosca E, et al. The role of extracellular matrix in mouse and human corneal neovascularization. *Sci Rep.* 2019;9:14272.
43. Chauhan SK, Dohlman TH, Dana R. Corneal lymphatics: role in ocular inflammation as inducer and responder of adaptive immunity. *J Clin Cell Immunol.* 2014;5:1000256.
44. Gurung HR, Carr MM, Carr DJ. Cornea lymphatics drive the CD8(+) T-cell response to herpes simplex virus-1. *Immunol Cell Biol.* 2017;95:87–98.
45. Avraham-Davidi I, Yona S, Grunewald M, et al. On-site education of VEGF-recruited monocytes improves their performance as angiogenic and arteriogenic accessory cells. *J Exp Med.* 2013;210:2611–2625.
46. Nakao S, Hafezi-Moghadam A, Ishibashi T. Lymphatics and lymphangiogenesis in the eye. *J Ophthalmol.* 2012;2012:783163.
47. Falcone DJ, McCaffrey TA, Haimovitz-Friedman A, Vergilio JA, Nicholson AC. Macrophage and foam cell release of matrix-bound growth factors. Role of plasminogen activation. *J Biol Chem.* 1993;268:11951–11958.
48. Enninga EAL, Chatzopoulos K, Butterfield JT, et al. CD206-positive myeloid cells bind galectin-9 and promote a tumor-supportive microenvironment. *J Pathol.* 2018;245:468–477.
49. Chen M, Bao L, Zhao M, Cao J, Zheng H. Progress in research on the role of FGF in the formation and treatment of corneal neovascularization. *Front Pharmacol.* 2020;11:111.
50. Araki-Sasaki K, Tanaka T, Ebisuno Y, et al. Dynamic expression of chemokines and the infiltration of inflammatory cells in the HSV-infected cornea and its associated tissues. *Ocul Immunol Inflamm.* 2006;14:257–266.
51. Conrady CD, Zheng M, Mandal NA, van Rooijen N, Carr DJ. IFN- α -driven CCL2 production recruits inflammatory monocytes to infection site in mice. *Mucosal Immunol.* 2013;6:45–55.
52. Jeon S, Rowe AM, Carroll KL, Harvey SAK, Hendricks RL. PD-L1/B7-H1 inhibits viral clearance by macrophages in HSV-1-infected corneas. *J Immunol.* 2018;200:3711–3719.
53. Hunt TK, Knighton DR, Thakral KK, Goodson WH, 3rd, Andrews WS. Studies on inflammation and wound healing: angiogenesis and collagen synthesis stimulated in vivo by resident and activated wound macrophages. *Surgery.* 1984;96:48–54.
54. Li S, Li B, Jiang H, et al. Macrophage depletion impairs corneal wound healing after autologous transplantation in mice. *PLoS One.* 2013;8:e61799.
55. Xue Y, He J, Xiao C, et al. The mouse autonomic nervous system modulates inflammation and epithelial renewal after corneal abrasion through the activation of distinct local macrophages. *Mucosal Immunol.* 2018;11:1496–1511.
56. Miyazaki K, Okada Y, Yamanaka O, et al. Corneal wound healing in an osteopontin-deficient mouse. *Invest Ophthalmol Vis Sci.* 2008;49:1367–1375.
57. Ashkar S, Weber GF, Panoutsakopoulou V, et al. Eta-1 (osteopontin): an early component of type-1 (cell-mediated) immunity. *Science.* 2000;287:860–864.
58. Rowe AM, St Leger AJ, Jeon S, Dhaliwal DK, Knickelbein JE, Hendricks RL. Herpes keratitis. *Prog Retin Eye Res.* 2013;32:88–101.
59. Thomas J, Kanangat S, Rouse BT. Herpes simplex virus replication-induced expression of chemokines and proinflammatory cytokines in the eye: implications in herpetic stromal keratitis. *J Interferon Cytokine Res.* 1998;18:681–690.
60. Gimenez F, Suryawanshi A, Rouse BT. Pathogenesis of herpes stromal keratitis—a focus on corneal neovascularization. *Prog Retin Eye Res.* 2013;33:1–9.
61. Rao P, Suvas PK, Jerome AD, Steinle JJ, Suvas S. Role of insulin-like growth factor binding protein-3 in the pathogenesis of herpes stromal keratitis. *Invest Ophthalmol Vis Sci.* 2020;61:46.
62. Murphy G, Nagase H. Progress in matrix metalloproteinase research. *Mol Aspects of Med.* 2008;29:290–308.
63. Bian F, Pelegriano FS, Henriksson JT, et al. Differential effects of dexamethasone and doxycycline on inflammation and MMP production in murine alkali-burned corneas associated with dry eye. *Ocul Surf.* 2016;14:242–254.
64. Astrom P, Pirila E, Lithovius R, et al. Matrix metalloproteinase-8 regulates transforming growth factor-beta1 levels in mouse tongue wounds and fibroblasts in vitro. *Exp Cell Res.* 2014;328:217–227.
65. Weber GF, Cantor H. The immunology of Eta-1/osteopontin. *Cytokine Growth Factor Rev.* 1996;7:241–248.
66. Singh R, Hui T, Matsui A, et al. Modulation of infection-mediated migration of neutrophils and CXCR2 trafficking by osteopontin. *Immunology.* 2017;150:74–86.
67. Dohlman TH, Yin J, Dana R. Methods for assessing corneal opacity. *Semin Ophthalmol.* 2019;34:205–210.